An Improved Real-Time Endovascular Guidewire Position Simulation Using Activity on Edge Network

Jianpeng Qiu, Libo Zhang, Guanyu Yang, Yang Chen, Shoujun Zhou

IEEE Access
Multidisciplinary | Rapid Review | Open Access Journal

Received June 27, 2019, accepted August 6, 2019, date of publication August 14, 2019, date of current version September 17, 2019.

Digital Object Identifier 10.1109/ACCESS.2019.2935327

An Improved Real-Time Endovascular Guidewire Position Simulation Using Activity on Edge Network

JIANPENG QIU[1],*, LIBO ZHANG[2],*, GUANYU YANG[1], YANG CHEN[1,3,4,5], (Senior Member, IEEE), AND SHOUJUN ZHOU[6]

[1]Laboratory of Image Science and Technology, School of Computer Science and Engineering, Southeast University, Nanjing 210096, China
[2]Radiology Department of the General Hospital of the Northern War Zone of the Chinese People's Liberation Army, Shenyang 110016, China
[3]Centre de Recherche en Information Biomedicale Sino-Francais (LIA CRIBs), 35000 Rennes, France
[4]Key Laboratory of Computer Network and Information Integration, Ministry of Education, Southeast University, Nanjing 210096, China
[5]School of Cyber Science and Engineering, Southeast University, Nanjing 210096, China
[6]Shenzhen Institutes of Advanced Technology, Chinese Academy of Sciences, Shenzhen 518055, China

Corresponding authors: Yang Chen (chenyang.list@seu.edu.cn) and Shoujun Zhou (sj.zhou@siat.ac.cn)
*Jianpeng Qiu and Libo Zhang are co-first authors.

This work was supported in part by the National Key Research and Development Program of China under Grant 2018YFA0704102, Grant 2017YFA0104302, Grant 2017YFC0109202, and Grant 2017YFC0107900, in part by the National High Technology Research and Development Program of China (863 Program), under Grant 2015AA043203, in part by the National Natural Science Foundation under Grant 81827805, Grant 61801003, Grant 61871117, and Grant 81530060, in part by the Shenzhen Engineering Laboratory for Key Technology on Intervention Diagnosis and Treatment Integration, in part by the Key Laboratory of Health Informatics, Chinese Academy of Sciences, in part by the Fundamental Research Funds for the Central Universities, in part by the Joint Research Project of Southeast University and Nanjing Medical University, in part by the Technical Product Research Project of Joint Logistic Support Force of Chinese PLA under Grant CLB18C050, and in part by the R&D Projects in Key Technology Areas of Guangdong Province under Grant 2018B030333001.

ABSTRACT A novel network-based method to realistically simulate the guidewire position in the vascular system is presented in this paper. We can always obtain an ideal guidewire path by the shortest path algorithm, particularly, critical path algorithm based on the principle of maximum path length. Besides, we propose an adaptive sampling algorithm and optimizations based on two ends of the guidewire to adjust the guidewire position toward achieving an ideal simulation result. Compared with previous results, we can achieve 29%, 20% and 47% improvements in accuracy for three phantoms under the same conditions.

INDEX TERMS
Endovascular interventions, guidewire simulation, real time, activity on edge network, critical path.

I. INTRODUCTION

Cardiovascular disease ranks first among all causes of death, resulting in more than 15 million deaths each year in the world. Over the past few decades, minimally invasive vascular intervention surgery has taken place rapid development with the advantages of faster recovery, smaller incisions, less blood loss, a shorter hospital stay and decreased pain. In this surgery, a flexible guidewire is first placed in the remote punctured artery site and navigated to the diseased site under fluoroscopic guidance. Physicians then gently move the devices, such as catheter, stents, balloons or coils, to the interventional site along the inserted guidewire, i.e., the guidewire is considered as a guide track for these devices.

The associate editor coordinating the review of this article and approving it for publication was Carmelo Militello.

This operation is complicated due to the guidewire's shape and position arbitrary change inside the vessel lumen. In addition, excessive force can lead to complications, such as hemorrhage, vessel spasm, or vessel plaque release [17]. Complications may occur especially in symptomatic and older patients, which often have weakened vessel structures with reduced flexibility and high calcification rates [19]. Hence, only interventional radiologists can perform the operation on real patients. It is valuable to predict the guidewire position in advance to optimize the image-guided procedure.

Some methods have been proposed to realistically simulate the behavior of a guidewire. To model bending, twists and other deformations, several groups have incorporated the connected beam elements into the finite element method (FEM), e.g. linear elastic [9], [10], [14] and static [6], [20] finite element representations. In addition,

some of the above methods have been used in the medical simulators, see, e.g., [2], [4], [6], [15]. Cotin *et al.* [5] presented a linear model based on the finite beam elements and substructure decomposition, their method allows nonlinear simulation. Konings *et al.* [1], [11], [12] presented the guidewire path as an energy function and minimized it in an iterative fashion. To avoid the high computational cost, Schafer *et al.* [18], [19], [21] expressed this problem as a shortest path algorithm of graph according to the analytical modeling ideas [3], [11] and beam-like FEM methods.

Based on the method of [18], [19], [21], Qiu *et al.* [16] provided an iterative refinement method to further reduce the computational cost. Based on the method of [18], [19], [21], Qiu *et al.* [16] provided an iterative refinement method to further reduce the computational cost. However, all the above methods cannot avoid the high computational cost and the failure to obtain an ideal simulation result within an acceptable time frame.

In this paper, we provide a new network-based method to simulate the behavior of a guidewire in the vascular system. The method adopts an adaptive sampling algorithm, an improved activity on edge (AOE) network method as well as an end-based optimization approach, improving both efficiency and accuracy in simulations.

The organization of the paper is as follows: the proposed method is presented in Section II. The experiment results and compares the proposed model with an existing model are presented in Section III**.** The experiment results are discussed in Section IV. Finally, the conclusion and indicates directions of future work are given in Section V.

II. PROPOSED METHOD

In this section, we propose a network-based method to simulate the guidewire path in the vascular system, our method involves the following main tasks. We first present an iterative refinement method based on the adaptive sampling algorithm to achieve some maximum curvature points, and use them to construct the AOE network. To assign a value to each directed edge on AOE network, an energy function is then defined. To calculate the critical path, we then discuss how to construct AOE network. Finally, we describe the optimization approach based on the front or back end of the simulated guidewire so as to optimize the simulation path.

A. ITERATIVE REFINEMENT ALGORITHM

In [16], Qiu *et al.* proposed an iterative refinement method but it cannot accurately identify some ordered centerline points with maximum curvature. To improve the accuracy of the point identification, the approach is improved by canceling the parameter α (number of maximum curvature's points) given in [16] and by adopting an adaptive sampling algorithm in this subsection.The centerline points (as the data input) are represented by an ordered set $L = \{L_0, \ldots L_{|L|-1}\}$, where $|L|$ denotes the size of set L. During the iterative refinement, we first identify a maximum curvature point between centerline points L_1 and $L_{|L|-2}$, and express it as L_{m} by using (1) [21].

$$C_{Lm} = \cos^{-1}\left(\overrightarrow{L_{i-5}L_i} \cdot \overrightarrow{L_iL_{i+5}}\right) \tag{1}$$

We then identify the maximum curvature points between L_1 and L_{m}, and between L_{m} and $L_{|L|-2}$, and so on. When the distance of centerline indexes of any two adjacent centerline points identified is less than a predefined constant δ (iterative refinement termination condition), we stop identifying the maximum curvature points. The indexes of the maximum curvature points generated during the iteration process constitute an ordered set C. We select the indexes of some maximum curvature points from set C according to the adaptive sampling algorithm (merge small edges) [13], and put them into ordered set B. Then, we identify several maximum curvature points according to a given threshold δ' ($\delta' > \delta$) and the adaptive sampling algorithm (split big edges) [13]. Finally, the centerline indexes of these points are put into the ordered set B.

The above steps can be described as follows:

Step 1: Put centerline indexes of L_1 and $L_{|L|-2}$ into set C, put centerline index of L_1 into set B;

Step 2: For any two points with consecutive indexes in the sorted set C (e.g., $L_{\mathrm{C[k]}}$ and $L_{\mathrm{C}[k+1]}$), we then generate the maximum curvature point (denoted by L_{m}) between $L_{\mathrm{C[k]}}$ and $L_{\mathrm{C}[k+1]}$ using (1) if the distance between them is more than δ (e.g., 3). The index m of this point is put into set C. Then, the set C is sorted in the increasing order of those index values. Step 2 is repeated until the distance between any two points with indexes in set C is less than δ;

Step 3: Filter an index of the maximum curvature point (denoted by L_h) from set C in the index range of [g + 5, g + 20] if g + 5 < $\mathrm{C_{[k]}}$ < g + 20, where g = 1, k = 0,1,2…|C| − 1. Otherwise, calculate a maximum curvature point (denoted by L_h) between L_{g+5} and L_{g+20} by $C_{Lh} = \cos^{-1}\left(\overrightarrow{L_{i-5}L_i} \cdot \overrightarrow{L_iL_{i+5}}\right)$. Then, the index h of this point is put into set B. Finally, g = h. Repeat Step 3 until g+ 5 > |L| − 2;

Step 4: Put centerline index of $L_{|L|-2}$ into ordered set B;

Step 5: If the distance of $\mathrm{B_{[k]}}$ and $\mathrm{B_{[k+1]}}$ is more than a given threshold δ'($\delta' > \delta$), get an index of another maximum curvature point between $\mathrm{B_{[k]}}$ and $\mathrm{B_{[k+1]}}$ by $C_{Li} = \cos^{-1}\left(\overrightarrow{L_{i-5}L_i} \cdot \overrightarrow{L_iL_{i+5}}\right)$, where $\mathrm{B_{[k]}} + 8 \le i \le \mathrm{B_{[k+1]}} - 8$, k = 0…|B| − 2. Then, The index of this point is put into set B. Step 5 is repeated until the distance between any two points with indexes in B is less than δ';

Step 6: Sort set B (e.g., using the quick sort algorithm);

Step 7: Get |B| ordered centerline points.

1) ILLUSTRATIVE EXAMPLE

Consider $L = \{L_0, \ldots, L_{35}\}$ with $\delta = 3$ and $\delta' = 8$.

Step 1: Put 1 and 34 into set C, put 1 in to set B;

Step 2: Generate the maximum curvature point denoted by L_{25} between L_1 and L_{34}. Then the maximum curvature points between L_1 and L_{25}, and between L_{25} and L_{34} are identified respectively, and so on. Put centerline indexes of these points

into set C and sort it to obtain C= {1, 4, 7, 10, 13, 15, 18, 20, 23, 25, 27, 28, 30, 31, 34};

Step 3: Filter an index 13 of the maximum curvature point L_{13} from set C in the index range of [1+5, 1+20], and put 13 into set B. Filter an index 25 of the maximum curvature point L_{25} in the index range of [13+5, 13+20], and put 25 into set B. Filter an index 31 of the maximum curvature point L_{31} in the index range of [25+5, 34], and put 31 into set B and obtain B = {1, 13, 25, 31};

Step 4: put 34 into set B and obtain B = {1, 13, 25, 31, 34};

Step 5: Since the distance between them is more than δ', generate maximum curvature points denoted by L_7 between L_1 and L_{13}, then generate maximum curvature points denoted by L_{20} between L_{13} and L_{25}. Finally, put 7 and 20 into set B and sort it to obtain B = {1, 7, 13, 20, 25, 31, 34}.

Upon completion of the iterative method, the ordered set B is obtained. Then, |B| meshes centered at each centerline point $L_{\mathrm{B[k]}}$ are constructed by using the same method as [16]. Each mesh $M_{L\mathrm{B[k]}}$ contains 4 circles and m sampled points (5–45 sampled points). Each sampled point is defined as $m_{i,L\mathrm{B[k]}}$, where i and $L_{\mathrm{B[k]}}$ refer to index of the sampled point on each mesh and index of each mesh, respectively.

Next, this spatial representation is represented as a network, i.e., |B| meshes and two endpoints of guidewire are denoted by an AOE network with |B|+2 layers. In this AOE network, the centerline points L_0 and $L_{|L|-1}$ are considered as the source point and meeting point, respectively. Each mesh $M_{L\mathrm{B[k]}}$ is represented as a layer. Each sampled point $m_i, L_{\mathrm{B[k]}}$ is considered as a node representing an event. Meanwhile, the directed edge connecting two sampled points is represented as an activity, its value is defined as the execution time of this activity. For each activity, its execution time, i.e., the value of the edge, is given by an energy function U that is defined in Section II.***B***. In addition, L_0 is connected to the first layer containing all sampled points of the first mesh and last layer containing all sampled points of the last mesh is connected to $L_{|\mathrm{B}|-1}$ respectively with 1 energy edges.

B. ENERGY FUNCTION

To better approximate the energy function for the guidewire, two types of energy are considered as shown in (2).

$$U = U_e + U_p \tag{2}$$

U_e in (2) is the elastic energy derived from the bending energy. It is first proposed by Bernoulli in 1738. Euler [7] studied intensively it for the case of planar curves. In our model, we accept the following definition of the bending energy reported in [16]. For any two consecutive sampled points $m_i, L_{\mathrm{B[k]}}$ and $m_r, L_{\mathrm{B[k-1]}}$, if $\cos_{(\theta 1)} = \cos\left(\overrightarrow{m_0, L_{\mathrm{B[k]}} - m_0, L_{\mathrm{B[k-1]}}} \cdot \overrightarrow{m_i, L_{\mathrm{B[k]}} - m_r, L_{\mathrm{B[k-1]}}}\right)$ and $\sin_{(\theta 2)} = \sin\left(\overrightarrow{m_0, L_{\mathrm{B[k-1]}} - m_r, L_{\mathrm{B[k-1]}}} \cdot \overrightarrow{m_i, L_{\mathrm{B[k]}} - m_r, L_{\mathrm{B[k-1]}}}\right)$, then

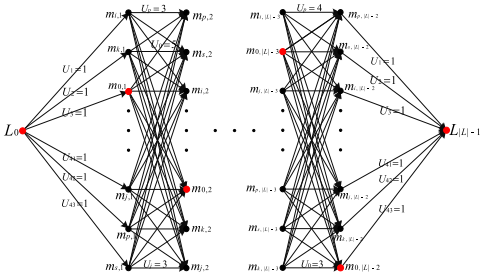

FIGURE 1. AOE network constructed by the energy function.

the elastic energy U_e is formulated as follow

$$U_e = \frac{1}{2}\left(\cos_{(\theta 1)}{}^2 + \sin_{(\theta 2)}{}^2\right) \tag{3}$$

U_p in (2) is the potential energy due to the distance from the sampled points $m_r, L_{\mathrm{B[k-1]}}$ and $m_0, L_{\mathrm{B[k-1]}}$. Therefore, we calculate it using Hooker's law [22] and define it as follow

$$U_p = \frac{1}{2}\left(R - \kappa \cdot ||m_r, L_{\mathrm{B[k-1]}} - m_0, L_{\mathrm{B[k-1]}}||\right), \tag{4}$$

where $||m_r, L_{\mathrm{B[k-1]}} - m_0, L_{\mathrm{B[k-1]}}||$, κ and R refer to the distance between $m_r, L_{\mathrm{B[k-1]}}$ and $m_0, L_{\mathrm{B[k-1]}}$, the curvature [8] at the sampled point $m_r, L_{\mathrm{B[k-1]}}$ and the vessel radius, respectively.

C. AOE NETWORK CONSTRUCTION

The AOE network is constructed as shown in Figure 1 once the energy value of each directed edge is defined using (2). The critical path with maximum path length on this network, i.e., shortest time to complete this project, is calculated using the following step-by-step process:

Step 1: The centerline points L_0 and $L_{|L|-1}$ are considered as source point and meeting point, respectively;

Step 2: Scramble serial number of the sampled points on each mesh $M_{L\mathrm{B[k]}}$;

Step 3: Calculate energy value of each directed edge according to the energy function (2);

Step 4: Start from the source point, calculate the earliest completion time of each node according to energy values of all in-degree edges of each node from source point to meeting point;

Step 5: The earliest completion time of meeting point $L_{|L|-1}$ is considered as shortest time to complete this project, i.e., maximum path length. Meanwhile, the meeting point $L_{|L|-1}$ is considered as the first critical node;

Step 6: Start from the meeting point $L_{|L|-1}$, calculate the latest completion time of each node according to energy values of all out-degree edges of each node from meeting point to source point. Meanwhile, the source point L_0 is considered as the last critical node;

Step 7: Calculate the critical node according to the earliest completion time and the latest completion time of each node. Then, record all critical nodes;

Step 8: Get |B|+2 critical nodes on the critical path.

TABLE 1. A group of simulation results for phantoms 1, 2 and 3.

Phantom number	RMS (mm)		Mesh number		*L* Length(points)	Vessel radius(mm)
	Proposed	Method in [14]	Proposed	Method in [14]		
1	0.4319	0.6060	59	52	563	6
2	0.4498	0.5646	54	52	498	8
3	0.4399	0.8331	41	41	384	6

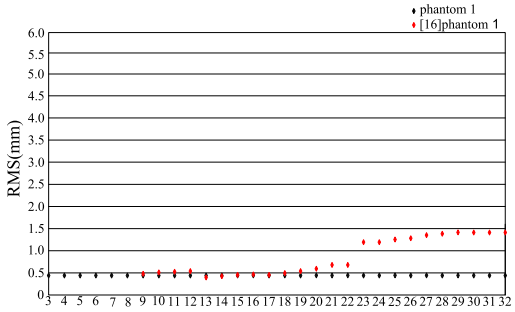

FIGURE 2. RMS vs. iterative termination conditions δ.

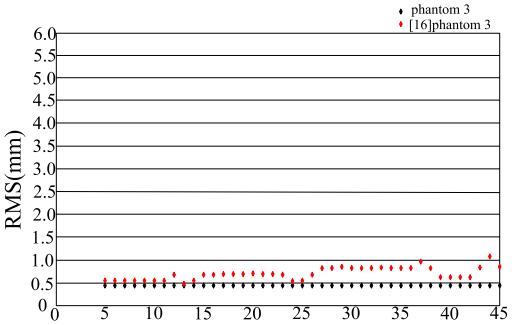

FIGURE 3. RMS vs. number of sampled points in each mesh.

D. OPTIMIZATION BASED ON TWO ENDS OF THE GUIDEWIRE

Upon completion of critical path on AOE network calculation, |B| +2 critical nodes are obtained. The interventional operation is likely to be affected by the implantation location and angle of guidewire. Therefore, we perform optimization based on two ends of the guidewire to reduce effects of this factor on the operation. We take the front-end optimization as an example since it is same as back-end optimization. The optimization steps can be described as the following step-by-step process:

Step 1: Compute a maximum curvature point L_k using (1), where $B_{[0]}+1 =< k <= B_{[1]} - 1$;

Step 2: Compute another maximum curvature point L_m using (1), where $k+1 =< m <= B_{[1]}-1$ or $B_{[0]} +1 =< m <= k - 1$;

Step 3: Compute the linear equation L_{ine} using (5):

$$\frac{x - x_1}{x_2 - x_1} = \frac{y - y_1}{y_2 - y_2} = \frac{z - z_1}{z_2 - z_1}, \tag{5}$$

where (x_1, y_1, z_1) and (x_2, y_2, z_2) refer to coordinates of the start point m_i, $L_{B[0]}$ and key node $L_{B[1]}$, respectively;

Step 4: Construct a mesh containing 16 circles by L_k, and construct a mesh containing 16 circles by L_m. Then, screen out an insertion point with the minimum vertical distance to the linear equation L_{ine} from the two meshes, respectively. Finally, this two insertion points are considered as critical nodes on critical path.

Finally, we calculate the simulation guidewire via cubic spline interpolation according to |B|+2 critical nodes and 4 insertion points generated from optimization based on two ends of the guidewire.

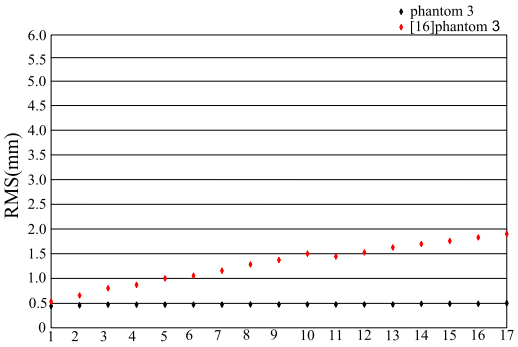

FIGURE 4. RMS vs. vessel radius for phantom 3.

III. RESULTS

The proposed method is evaluated by comparing simulation result *Gs* with reference guidewire *Gr*. For each point *i* in G_r, the closest point *j* in G_s is determined (6).

$$d_{rs}(i) = \min\left(G_r(i) - G_s(j)\right) \tag{6}$$

As an error measure, the root-mean-square (RMS) distance between G_s and G_r is determined. For a guidewire with N centerline points, the error measure is defined as follows:

$$RMS_{rs} = \sqrt{\frac{1}{N}\sum_{i}^{N}(d_{rs}(i))^2} \tag{7}$$

A. PERFORMANCE COMPARISION

Table 1 shows our simulation results. Parameter δ (iterative refinement termination condition) is equal to 5 and 20 in the proposed model and model of [16], respectively.

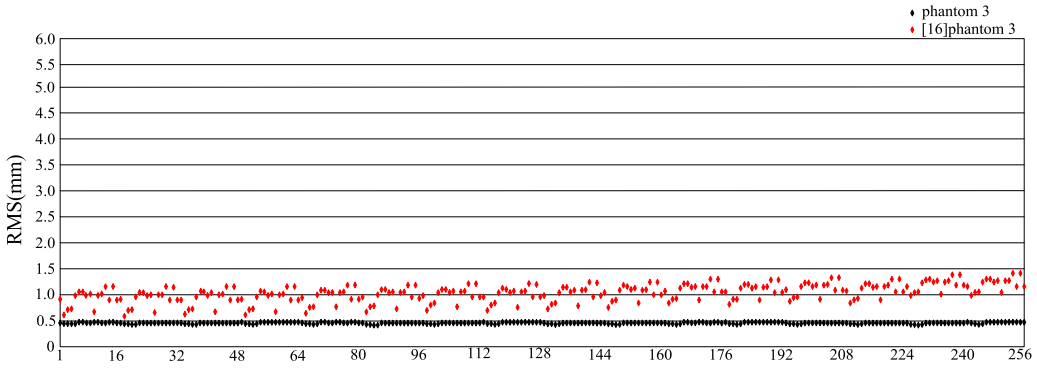

FIGURE 5. RMS vs. 256 simulations for possible combinations of start and end points in phantom 3.

Besides, each mesh contains 43 sampled points, the start point L_1 and end point $L_{|L|-2}$ are kept fixed. The length of the reference guidewire and vessel radius are also given in the last two columns of Table 1. Compared to [16] (using parameter $\alpha = 10$, representing the number of maximum curvature's points), we can achieve 29%, 20% and 47% improvements for phantoms 1, 2 and 3, respectively. In addition, our method can achieve better improvements in accuracy for three phantoms when parameter δ is more than 20, e.g., we can achieve 68%, 50% and 57% improvements for the three phantoms under the same conditions when δ is equal to 27.

B. EFFECTS OF PARAMETER δ

For this experiment, we keep the same parameters as those for generating results in Table 1 and only change value of parameter δ in the range of [3], [32]. Figure 2 shows that the RMS value using the proposed model is a constant 0.4319, while the RMS under the model of [16] are very unstable and vary from 0.3842 to 1.4128.

C. EFFECTS OF THE NUMBER OF SAMPLED POINTS

We keep the same parameters as those for generating results in Table 1 and only change the number of sampled points. Figure 3 shows that the RMS value under the proposed model is a constant 0.4399, while the RMS under the model of [16] are unstable and vary from 0.4946 to 1.0726.

D. EFFECTS OF THE VESSEL RADIUS

In this experiment, the same parameters as those for generating results in Table 1 are maintained and only change the size of the vessel radius. Then, we always calculate the critical path between sampled point $m_{42,1} \in M_1$ and sampled point $m_{42,|B|} \in M_{|B|}$. Figure 4 shows that the RMS values under the proposed model are almost all lower than 0.5 mm and almost unchanged, while the RMS under the model of [16] are larger and vary from 0.5486 to 1.9047.

E. EFFECTS OF START AND END POINTS

In this experiment, the same parameters as those for generating results in Table 1 and only change the start point $m_{0,1} \in M_1$) and end point $m_{0,|B|} \in M_{|B|}$), respectively. The 16 sampled points obtained from the meshes M_1 and $M_{|B|}$ respectively are considered as the start points and end points, respectively. Figure 5 shows that the RMS values under the proposed model are all lower than 0.5 mm and almost constant, while the RMS under the model of [16] are very unstable and vary from 0.5846 to 1.3949.

To further test whether the proposed model is affected by the selection of parameter of iterative refinement approach. Here, parameter α is equal to 8 under the model of [16]. Figure 6 shows the comparison results using a different value of parameter δ (= 26). The RMS values under the proposed model are all lower than 0.5 mm and almost unchanged, while the RMS values obtained using the model of [16] are almost all bigger than 1 mm.

F. RUNNING TIME

In this experiment, 50 running times are collected on quad-core computer with 4G memory. Compare to the model of [16], Table 2 shows the proposed model has a shorter running time.

IV. DISCUSSION

Based on our simulation study in Section III.***B***, the statistical data collected using different values of δ show our RMS difference obtained using the proposed model is equal to 0 mm, whereas it is $\leq$ 1.0286 mm under the model of [16] for phantom 1. Similar simulations can be obtained for phantoms 2 and 3. Therefore, the simulation results are not affected by the selection of parameter δ of the iterative refinement approach.

Based on our study on the number of sampled points in Section III.***C***, the statistical data show our RMS difference obtained using the proposed model is equal to 0 mm, whereas it is $\leq$ 0.5780 mm under the model of [16] for phantom 3. Similar situation can be obtained for phantoms 1 and 2. Therefore, the simulation results are not affected by the number of sample points adopted.

Based on our study on the vessel radius in Section III.***D***, the statistical data show our RMS difference obtained using

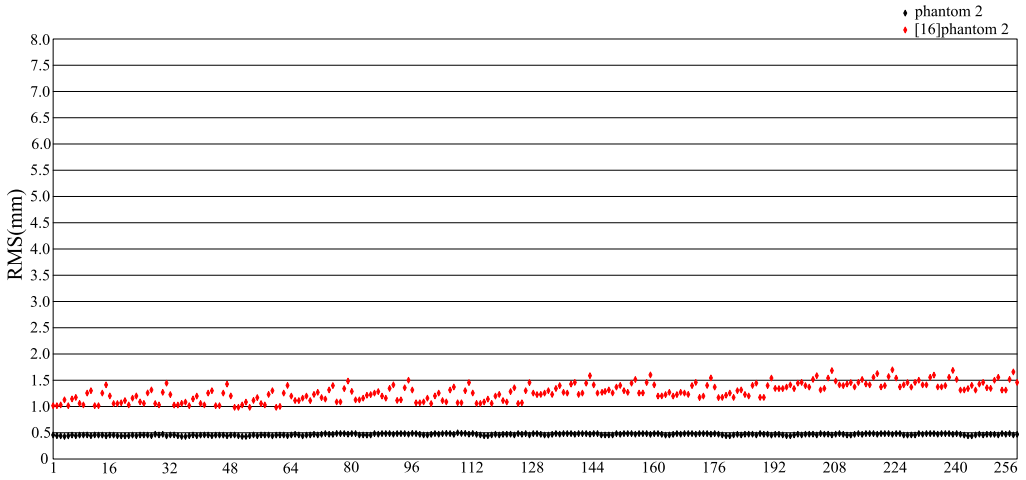

FIGURE 6. RMS vs. 256 simulations for possible combinations of start and end points in phantom 2.

TABLE 2. Statistics of 50 running times (in seconds) for phantoms 1, 2, and 3.

Phantom number	The proposed model			Model of [16]		
	Long time	Shortest time	Mean time	Long time	Shortest time	Mean time
1	0.2810	0.1540	0.1615	4.8040	4.6020	4.6977
2	0.2419	0.1400	0.1518	4.9120	4.6530	4.7627
3	0.1250	0.1090	0.1182	5.8060	4.8912	5.1019

the proposed model is $\leq$ 0.0632 mm, whereas it is $\leq$ 1.3561 mm under the model of [16] for phantom 3. Similar situation can be obtained for phantoms 1 and 2. Therefore, the simulation results are only slightly affected by the change of vessel radius, such as vessel expansion and constriction.

Based on our study on the start and end points in Section III.***E***. In Figure 5, the statistical data show our RMS difference obtained using the proposed model is $\leq$ 0.0461 mm, whereas it is $\leq$ 0.8103 mm under the model of [16] for phantom 3. Similar comparison result can be made for phantoms 1 and 2. Therefore, the proposed method is more robust to the position and angle of the start and end points. In Figure 6, we still obtain a similar comparison result using a different value of parameter δ for phantom 2.

V. CONCLUSION AND FUTURE WORK

In this paper, we have proposed a novel network-based method to simulate the guidewire path for surgical operations. The proposed method improves the iterative refinement procedure by canceling the parameter α of the existing work [16] and by adopting an adaptive sampling algorithm. The optimal path is determined based on the AOE network method and the optimization approach based on two ends of the guidewire. Simulation results indicate that the proposed method presents more accurate and faster running time than the existing method of [16]. In the future, we would like to incorporate vascular deformation into the proposed method.

ACKNOWLEDGMENT

The authors thank the Yong Tian from School of Information Science and Engineering of Lanzhou University for providing the original data.

REFERENCES

[1] T. Alderliesten, P. A. N. Bosman, and W. J. Niessen, "Towards a real-time minimally-invasive vascular intervention simulation system," *IEEE Trans. Med. Imag.*, vol. 26, no. 1, pp. 128–132, Jan. 2007.

[2] T. Alderliesten, M. K. Konings, and W. J. Niessen, "Simulation of minimally invasive vascular interventions for training purposes," *Comput. Aided Surg.*, vol. 9, nos. 1–2, pp. 3–15, 2004.

[3] T. Alderliesten, M. K. Konings, and W. J. Niessen, "Modeling friction, intrinsic curvature, and rotation of guide wires for simulation of minimally invasive vascular interventions," *IEEE Trans. Biomed. Eng.*, vol. 54, no. 1, pp. 29–38, Jan. 2007.

[4] Y. Cai, C. Chui, X. Ye, Y. Wang, and J. H. Anderson, "VR simulated training for less invasive vascular intervention," *Comput. Graph.*, vol. 27, no. 2, pp. 215–221, Apr. 2003.

[5] S. Cotin, C. Duriez, J. Lenoir, P. Neumann, and S. Dawson, "New approaches to catheter navigation for interventional radiology simulation," in *Medical Image Computing and Computer-Assisted Intervention—MICCAI*. Berlin, Germany: Springs, 2005, pp. 534–542.

[6] S. L. Dawson, S. Cotin, D. Meglan, D. W. Shaffer, and M. A. Ferrell, "Designing a computer-based simulator for interventional cardiology training," *Catheterization Cardiovascular Interventions*, vol. 51, no. 4, pp. 522–527, 2000.

[7] L. Euler, *Methodus Inveniendi Lineas Curvas Maximi Minimive Proprietate Gaudentes Sive Solutio Problematis Isoperimetrici Latissimo Sensu Accepti*, C. Carathéodory, Ed. Lausanne, Switzerland: Marc-MichelBousquet & Co., 1952.

[8] J. A. Thorpe, *Elementary Topics in Differential Geometry*. New York, NY, USA: Springer-Verlag, 1979.

[9] J. Gindre, A. Bel-Brunon, M. Rochette, A. Lucas, A. Kaladji, P. Haigron, and A. Combescure, "Patient-specific finite-element simulation of the insertion of guidewire during an EVAR procedure: Guidewire position prediction validation on 28 cases," *IEEE Trans. Biomed. Eng.*, vol. 64, no. 5, pp. 1057–1066, May 2017.
[10] J. Gindre, A. Bel-Brunon, A. Kaladji, A. Duménil, M. Rochette, A. Lucas, P. Haigron, and A. Combescure, "Finite element simulation of the insertion of guidewires during an EVAR procedure: Example of a complex patient case, a first step toward patient-specific parameterized models," *Int. J. Numer. Methods Biomed. Eng.* vol. 31, no. 7, 2015, Art. no. e02716.
[11] M. K. Konings, E. B. van de Kraats, T. Alderliesten, and W. J. Niessen, "Analytical guide wire motion algorithm for simulation of endovascular interventions," *Med. Biol. Eng. Comput.*, vol. 41, no. 6, pp. 689–700, Nov. 2003.
[12] P. Landwehr, R. Schindler, U. Heinrich, W. Dölken, T. Krahe, and K. Lackner, "Quantification of vascular stenosis with color Doppler flow imaging: *In vitro* investigations," *Radiology* vol. 178, no. 3, pp. 701–704, 1991.
[13] M. Luo, H. Xie, L. Xie, P. Cai, and L. Gu, "A robust and real-time vascular intervention simulation based on Kirchhoff elastic rod," *Comput. Med. Imag. Graph.*, vol. 38, no. 8, pp. 735–743, Dec. 2014.
[14] W. L. Nowinski and C.-K. Chui, "Simulation of interventional neuroradiology procedures," in *Proc. Int. Workshop Med. Imag. Augmented Reality*, Jun. 2001, pp. 87–94.
[15] P. Korzeniowski, R. J. White, and F. Bello, "VCSim3: A VR simulator for cardiovascular interventions," *Int. J. Comput. Assist. Radiol. Surg.*, vol. 13, no. 1, pp. 135–149, Jan. 2018.
[16] J. Qiu, Z. Qu, H. Qiu, and X. Zhang, "An improved real-time endovascular guidewire position simulation using shortest path algorithm," *Med. Biol. Eng. Comput.*, vol. 54, no. 9, pp. 1375–1382, Sep. 2016.
[17] G. S. Roubin, S. Iyer, A. Halkin, J. Vitek, and C. Brennan, "Realizing the potential of carotid artery stenting: Proposed paradigms for patient selection and procedural technique," *Circulation*, vol. 113, no. 16, pp. 2021–2030, 2006.
[18] S. Schafer, V. Singh, K. R. Hoffmann, P. B. Noël, and J. Xu, "Planning image-guided endovascular interventions: Guidewire simulation using shortest path algorithms," *Proc. SPIE*, vol. 6509, Mar. 2007, Art. no. 65092C.
[19] S. Schafer, V. Singh, P. B. Noël, A. M. Walczak, J. Xu, and K. R. Hoffmann, "Real-time endovascular guidewire position simulation using shortest path algorithms," *Int. J. Comput. Assist. Radiol. Surg.*, vol. 4, no. 6, pp. 597–608, Nov. 2009.
[20] Y. P. Wang, C. K. Chui, Y. Y. Cai, and K. H. Mak, "Topology supported finite element method analysis of catheter/guidewire navigation in reconstructed coronary arteries," in *Proc. Comput. Cardiol.*, vol. 24, Sep. 1997, pp. 529–532.
[21] L. Xu, Y. Tian, X. Jin, J. Chen, S. Schafer, K. Hoffmann, and J. Xu, "An improved endovascular guidewire position simulation algorithm," in *Proc. 9th IEEE Int. Symp. Biomed. Imag.*, May 2012, pp. 1196–1199.
[22] T. X. Yu and L. C. Zhang, *Plastic Bending: Theory and Applications*. Singapore: World Scientific, 1996.

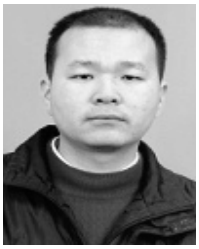

JIANPENG QIU is currently pursuing the Ph.D. degree in software engineering with Southeast University. His research interests include biomedical engineering, multimedia information processing, and medical image processing.

LIBO ZHANG received the M.S. and Ph.D. degrees in biomedical engineering from Northeastern University, China, in 2011 and 2016, respectively. Since 2016, he has been a Faculty Member with the Radiology Department of the General Hospital of the Northern War Zone of the Chinese People's Liberation Army (PLA). His research interests include medical image reconstruction, image analysis, and computer-aided diagnosis.

GUANYU YANG received the B.S. and M.S. degrees in biomedical engineering from Southeast University, Nanjing, China, in 2002 and 2005, respectively, and the Ph.D. degree in signal and image processing from the University of Rennes, Rennes, France, in 2009. He is currently an Associate Professor with the School of Computer Science and Engineering, Southeast University, Nanjing. His research interests include medical image processing and computer-assisted systems for diagnosis and therapy in medicine.

YANG CHEN received the M.S. and Ph.D. degrees in biomedical engineering from First Military Medical University, China, in 2004 and 2007, respectively. Since 2008, he has been a Faculty Member with the Department of Computer Science and Engineering, Southeast University, China. His research interests include medical image reconstruction, image analysis, pattern recognition, and computer-aided diagnosis.

SHOUJUN ZHOU received the M.S. degree from the School of Information, Lanzhou University, China, in 2001, and the Ph.D. degree in biomedical engineering from First Military Medical University, China, in 2004. Since 2010, he has been a Faculty Member with the Shenzhen Institutes of Advanced Technology, Chinese Academy of Sciences, China. His research interests include medical image analysis, pattern recognition, and computer-aided diagnosis and therapy.